Thermodynamics and Kinetics of Leaching High Alkali Red Mud with Dilute Sulfuric Acid

Chao Tang[1], Xingyu Hu[2], Hua Zeng[3], Jianfei Zhou[4] and Li Wang[5]
1. PhD student
2.Postgraduate Researcher
3.PhD student
4.PhD student
5.Professor
Central South University, China
Corresponding author: li_wang@csu.edu.cn; 5284woaifazi@163.com
https://doi.org/10.71659/icsoba2025-br009

Abstract

This study conducted an in-depth analysis of the thermodynamic and kinetic characteristics during the sulfuric acid leaching process of high-alkali red mud, aiming to optimize leaching parameters for efficient recovery of valuable components. Thermodynamic analysis revealed that the Gibbs free energy change (ΔG_T°) for Fe_2O_3 and Al_2O_3 leaching reactions increases with rising temperature, inhibiting their dissolution, whereas the ΔG_T° values for Na_2O and CaO decrease with temperature elevation, indicating enhanced leaching efficiency for these two components. Specifically, the Fe_2O_3 leaching reaction becomes non-spontaneous above 309 K, while Na_2O demonstrates the strongest leaching tendency and would be preferentially extracted. By controlling temperature and pH in the leaching system, selective extraction of components can be optimized. For instance, Na_2O can be individually leached at temperatures exceeding 323 K with pH maintained between 4.0 to 7.0. Kinetic analysis showed that sulfuric acid reacts completely with most sodium-containing compounds in red mud within 10 minutes at 298 K or 5 minutes at 323–348 K, achieving sodium leaching rates approaching 99 %. Model fitting indicated that the leaching process is predominantly controlled by mixed mechanisms involving both internal diffusion and chemical reactions, with the optimal kinetic function described as 1/3ln(1-x)-1+(1-x)-1/3. The calculated apparent activation energy of 12.07 kJ/mol further corroborated this conclusion. This research provides theoretical foundations for efficient high-alkali red mud leaching and contributes to promoting its sustainable utilization in industrial applications.

Keywords: High alkali red mud, Dilute sulfuric acid leaching, Leaching thermodynamics, Leaching kinetics.

1. Introduction

Red mud, an alkaline byproduct generated during the bauxite refining process, exhibits a high pH ranging from approximately 10 to 12.5 [1]. It contains substantial concentrations of heavy metals (e.g., Cd and Cr), radioactive elements (including Th, Hf, U, and rare earth elements), as well as fluorides[1–11]. Owing to its elevated alkalinity and heavy metal content, the stockpiling of red mud not only requires extensive land occupation but also poses environmental risks due to the leaching of contaminants, which can adversely affect surrounding soil and groundwater [12, 13]. Acid neutralization, as one of the most common methods for red mud alkali removal, is characterized by high solid-liquid separation efficiency and thorough alkali removal. Under appropriate conditions, the dealkalization rate can exceed 95 %. However, this method consumes a significant amount of acid, making the identification of suitable waste acids to reduce costs or the recovery of valuable elements critical for its efficient industrial application [14].

This study addresses the challenge of strong alkalinity in red mud from current alumina industrial production systems. By utilizing titanium white waste acid as a neutralizing agent for red mud and calcium-based salts as auxiliary additives in the acid leaching dealkalization process, it achieves directional regulation of silicate and metal ion dissolution and migration behaviours. The research provides theoretical and technical support for the comprehensive utilization of red mud, thereby helping to resolve the environmental pollution and safety issues caused by red mud in aluminium smelting. Meanwhile, this study is dedicated to an in-depth thermodynamic analysis of the leaching process, aiming to establish a solid theoretical foundation for leaching experiments and elucidate the response mechanisms of leaching reactions to variations in solution composition and environmental conditions. Through systematic investigation of these thermodynamic properties, we can precisely guide experimental design and optimize operational parameters. The ultimate objectives are to enhance leaching efficiency while minimizing energy consumption and environmental impact, thereby contributing to more sustainable and environmentally friendly industrial production practices.

2. Computational Analysis and Research Methods

2.1 Thermodynamic Calculation

The branch of thermodynamic analysis in chemical thermodynamics focuses on investigating the spontaneity, directionality, and limits of chemical reactions. This discipline establishes theoretical models and conducts quantitative analyses to predict the feasibility and extent of chemical reactions under specific conditions, thereby providing theoretical support for experimental design. The application of thermodynamic principles to experimental practice helps reduce uncertainties in experimental exploration and optimize experimental protocols, consequently enhancing both the efficiency and scientific rigor of experiments.

HSC Chemistry (by Metso) is a powerful thermochemical analysis software that integrates comprehensive functionalities in general chemistry, thermodynamics, and mineral processing. The software features an extensive thermochemical database encompassing thermodynamic properties (enthalpy (H), entropy (S), and heat capacity (C)) of more than 29 000 compounds. It also incorporates multiple computational modules, including process simulation, reaction equations, heat and material balances, and E-pH diagrams (also known as Pourbaix diagrams).

The E-pH diagram module provides a clear visualization of element speciation in specific aqueous media, delineating the conditions under which reactions proceed spontaneously and identifying stability domains for various species in aqueous solutions. Such diagrams are indispensable for understanding and predicting the chemical behaviour of metals under diverse environmental conditions.

2.2 Kinetic Calculation

Leaching kinetics, as an important branch of chemical kinetics, focuses on studying the rates and influencing factors of chemical reactions during leaching processes. By constructing kinetic models for leaching systems and employing various experimental techniques and mathematical methods for quantitative analysis, it reveals the intrinsic mechanisms of leaching reactions. This enables a deeper understanding of rate-limiting steps at different stages of the reaction process, such as diffusion control and chemical reaction control, as well as the degree of influence of factors like temperature, concentration, particle size, and agitation intensity on leaching rates. Applying leaching kinetics theory to actual production allows for precise regulation of leaching process parameters, improving leaching efficiency and selectivity, reducing costs, and achieving efficient resource utilization and environmentally friendly industrial production.

3. Result Analysis and Discussion

3.1 Thermodynamic Analysis

3.1.1 The Effect of Temperature on ΔG

The main components of the high-alkalinity red mud used in this experiment include Fe_2O_3, Al_2O_3, SiO_2, Na_2O, TiO_2, and CaO. The standard Gibbs free energy (ΔG^o) thermodynamic data of the reactants at 298 K during sulfuric acid leaching are also presented in Table 1.

Table 1. Thermodynamic data of reactants in leaching process at 298 K.

Materials	H°_{298}/(kJ/mol)	G°_{298} (kJ/mol)	S°_{298} (J/mol·K)
Fe_2O_3	-823.00	-846.36	78.40
Al_2O_3	-1675.69	-1690.87	50.95
SiO_2	-910.86	-923.22	41.46
Na_2O	-415.10	-437.46	75.04
TiO_2	-944.75	-959.74	50.29
CaO	-634.92	-646.27	38.10
H_2O(l)	-285.83	-306.68	69.95
H_2SO_4(l)	-788.34	-868.81	270.03

The chemical equations that may exist during the leaching process are as follows:

$$Fe_2O_3(s) + 6H^+ = 2Fe^{3+}(aq) + 3H_2O(l) \quad (1)$$

$$Al_2O_3(s) + 6H^+ = 2Al^{3+}(aq) + 3H_2O(l) \quad (2)$$

$$Na_2O(s) + 2H^+ = 2Na^+(aq) + 3H_2O(l) \quad (3)$$

$$CaO(s) + 2H^+ + SO_4^{2-} = CaSO_4\downarrow + H_2O(l) \quad (4)$$

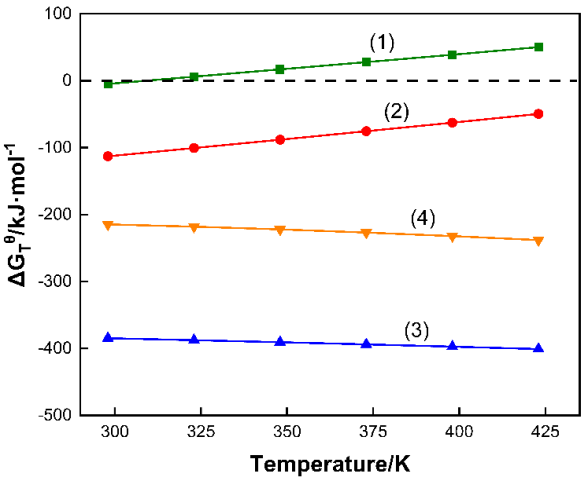

Figure 1. ΔG°_T of various reaction formulas at different specific temperatures.

Based on the standard Gibbs free energy (G^o) at specified temperatures (298 K, 323 K, 348 K, 373 K) provided in the Handbook of Inorganic Thermodynamics, the standard Gibbs free energy changes (ΔG°_T) for reactions (1) to (4) at these temperatures were calculated. The obtained data

were then subjected to univariate quadratic linear fitting to derive ΔG_T° functions for each reaction in the high-alkalinity red mud leaching process, as presented in Tables 2 and 3, and Figure 1.

Table 2. ΔG_T° of chemical equations (1–4).

Equation	ΔG_T° (kJ/mol)					
	298 K	323 K	348 K	373 K	398 K	423 K
(1)	-4.75	6.08	16.95	27.88	38.95	50.26
(2)	-112.90	-100.55	-88.07	-75.46	-62.64	-49.52
(3)	-384.64	-387.53	-390.60	-393.86	-397.29	-400.86
(4)	-214.62	-218.0	-222.07	-226.76	-232.08	-238.03

Table 3. ΔG_T° function of chemical equations (1–4).

Equation	ΔG_T° fitting function	R^2
(1)	$-124.174 + 0.3736\ T + 9.1429\times10^{-5}\ T^2$	0.999
(2)	$-245.0641 + 0.3992\ T + 1.4886\times10^{-4}\ T^2$	1
(3)	$-363.3632 - 0.0302\ T - 1.3829\times10^{-4}\ T^2$	1
(4)	$-223.0503+0.1803T-5.1\times10^{-4}T^2$	1

As shown in Table 3, the correlation coefficients (R^2) of the ΔG_T° fitting functions for all substances exceed 0.99, indicating excellent fitting results. From Table 2 and Figure 1, it can be observed that when the leaching temperature ranges from 298 K to 423 K, the ΔG_T° for the reaction between Fe_2O_3 and sulfuric acid gradually increases to positive values. Through calculation using the ΔG_T° fitting function, it is determined that when the leaching temperature exceeds 309 K, the ΔG_T° for the reaction between Fe_2O_3 and sulfuric acid becomes greater than 0, indicating the reaction cannot proceed spontaneously. In contrast, the ΔG_T° values for the other three possible reactions remain negative throughout this temperature range, suggesting these leaching reactions can occur spontaneously.

Furthermore, the analysis reveals that as temperature increases:

- The ΔG_T° values for reactions of Fe_2O_3 and Al_2O_3 with sulfuric acid gradually increase, demonstrating that higher temperatures are unfavourable for their dissolution;
- The ΔG_T° values for Na_2O and CaO leaching reactions progressively decrease, indicating enhanced leaching efficiency at elevated temperatures.

Notably, the comparison of reaction Equation (3) with others shows that Na_2O leaching exhibits significantly lower ΔG_T° values. According to thermodynamic principles, more negative ΔG_T° values correspond to greater spontaneous reaction tendencies. Therefore, during dilute sulfuric acid leaching of high-alkalinity red mud, Na_2O, with its stronger leaching tendency, will be preferentially extracted.

The magnitude of the equilibrium constant (K_a) reflects the feasibility of the reaction. Based on Equation (5):

$$\Delta G_T^\circ = -RT \ln K_a \tag{5}$$

the K_a values at different temperatures were calculated stepwise, with the results presented in Table 4.

When the equilibrium constant (K_a) exceeds 10^5, the reaction proceeds nearly to completion, whereas when K_a falls below 10^{-5}, the reaction becomes thermodynamically unfavourable. As evidenced by Table 4, with the exception of the Fe_2O_3 leaching reaction, all other reactions exhibit

K_a values greater than 10^5 across the studied temperature range. This indicates that the leaching of Al_2O_3, Na_2O, and CaO achieves near-complete conversion under these conditions.

Table 4. Equilibrium constants K_a of various reaction equations at different temperatures.

Equation	K_a					
	298 K	323 K	348 K	373 K	398 K	423 K
(1)	$10^{0.83}$	$10^{-0.98}$	$10^{-2.54}$	$10^{-3.9}$	$10^{-5.11}$	$10^{-6.21}$
(2)	$10^{19.78}$	$10^{16.25}$	$10^{13.22}$	$10^{10.56}$	$10^{8.22}$	$10^{6.11}$
(3)	$10^{67.39}$	$10^{62.65}$	$10^{58.61}$	$10^{55.14}$	$10^{52.13}$	$10^{49.49}$
(4)	$10^{37.6}$	$10^{35.24}$	$10^{33.32}$	$10^{31.75}$	$10^{30.45}$	$10^{29.39}$

Notably, when the temperature surpasses 398 K, the K_a for the Fe_2O_3-sulfuric acid reaction drops below 10^{-5}, rendering the reaction effectively non-viable. Furthermore, Reaction (3) consistently demonstrates higher K_a values compared to the other three reactions, thermodynamically confirming that Na_2O undergoes preferential and exhaustive leaching dissolution in this process.

3.1.2 The Effect of pH on ΔG

In leaching reactions, the pH value exerts a critical influence on the Gibbs free energy change (ΔG). Variations in pH directly affect:

- the stability of reactants and products;
- the regulation of reaction rates and equilibria;
- the interfacial reactions and dissolution-precipitation processes.

These collective effects fundamentally determine the ΔG of leaching reactions, thereby governing their spontaneity. Consequently, pH stands as a pivotal control parameter in leaching systems.

In the current experiment, the reactions for dilute sulfuric acid leaching of high-alkalinity red mud are represented by Equations (1–4). Notably, the leaching of Fe_2O_3 and Al_2O_3 requires precise condition control, as the generated Fe^{3+} and Al^{3+} ions are prone to hydrolysis and subsequent re-precipitation into the residue.

Figure 2 presents the E-pH diagrams of the Fe-H_2SO_4-H_2O leaching system at different temperatures (298 K, 348 K, 398 K). The results demonstrate that at 298 K and pH = 0.1, Fe_2O_3 can be dissolved by sulfuric acid to form Fe^{3+} ions. However, this dissolution becomes thermodynamically unfavourable at elevated temperatures.

These experimental observations are in excellent agreement with the thermodynamic calculations in Section 3.1.1, which predicted that the leaching reaction between Fe_2O_3 and sulfuric acid becomes non-spontaneous ($\Delta G_T^\circ > 0$) when the temperature exceeds 309 K. The combined results clearly indicate that the effective leaching of Fe_2O_3 requires strictly controlled conditions, specifically:

- low temperature operation (< 309 K)
- highly acidic environment (pH ≤ 0.1)
- proper redox potential maintenance

The stringent requirements for Fe_2O_3 leaching contrast sharply with the more favourable leaching behaviour of other components (Al_2O_3, Na_2O, CaO) in the red mud system, highlighting the need for selective leaching strategies in process design.

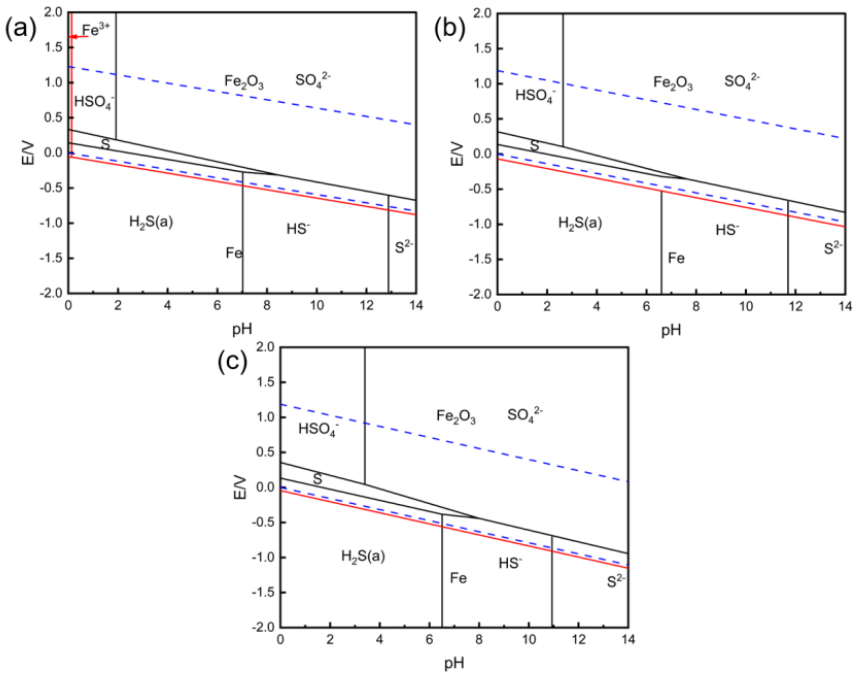

Figure 2. E-pH diagram of leaching reactions in Fe-H_2SO_4-H_2O system at different temperatures. (a): 298 K, (b): 348 K, (c): 398 K.

Figure 3 presents the E-pH diagrams of the Al-H_2SO_4-H_2O ternary leaching system at temperatures of 298 K, 348 K and 398 K. The results indicate that the reaction between Al_2O_3 and sulfuric acid can proceed spontaneously within the temperature range of 298 K to 398 K. At 298 K, the leaching reaction of Al_2O_3 requires a solution pH of 3.3, while at elevated temperatures of 348 K and 398 K, the pH values required to dissolve Al_2O_3 into Al^{3+} decrease to 2.2 and 1.9, respectively. This demonstrates that the required pH for the leaching reaction progressively decreases with increasing temperature, indicating more stringent reaction conditions.

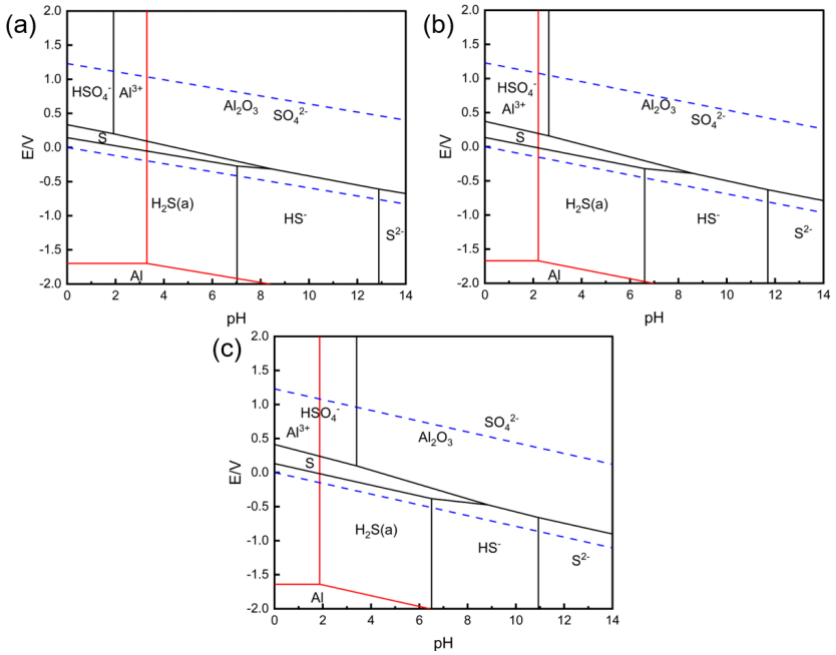

Figure 3. E-pH diagram of leaching reactions in Al-H_2SO_4-H_2O system at different temperatures. (a): 298 K, (b): 348 K, (c): 398 K.

This phenomenon can be attributed to the continuous increase in ΔG_T° of the reaction with rising temperature, leading to a gradual reduction in reaction spontaneity. These experimental observations are in good agreement with the thermodynamic calculations presented in -previous section, confirming the temperature-dependent characteristics of Al_2O_3 leaching behaviour in sulfuric acid solutions. The results suggest that while Al_2O_3 leaching remains thermodynamically favourable across this temperature range, the process becomes increasingly demanding at higher temperatures due to the need for stronger acidic conditions.

Following complete dissolution of Fe_2O_3 and Al_2O_3 by sulfuric acid leaching, Fe^{3+} and Al^{3+} ions enter the aqueous solution. Given their susceptibility to hydrolysis, the pH-dependent hydrolysis behaviour of these ions requires careful consideration. Figure 4 presents the E-pH diagrams of the Fe-H_2SO_4-H_2O hydrolysis system at temperatures of 298 K, 348 K, and 398 K. The results demonstrate that after complete reaction between Fe_2O_3 and sulfuric acid, iron primarily exists as Fe^{3+} and $Fe(OH)_3$.

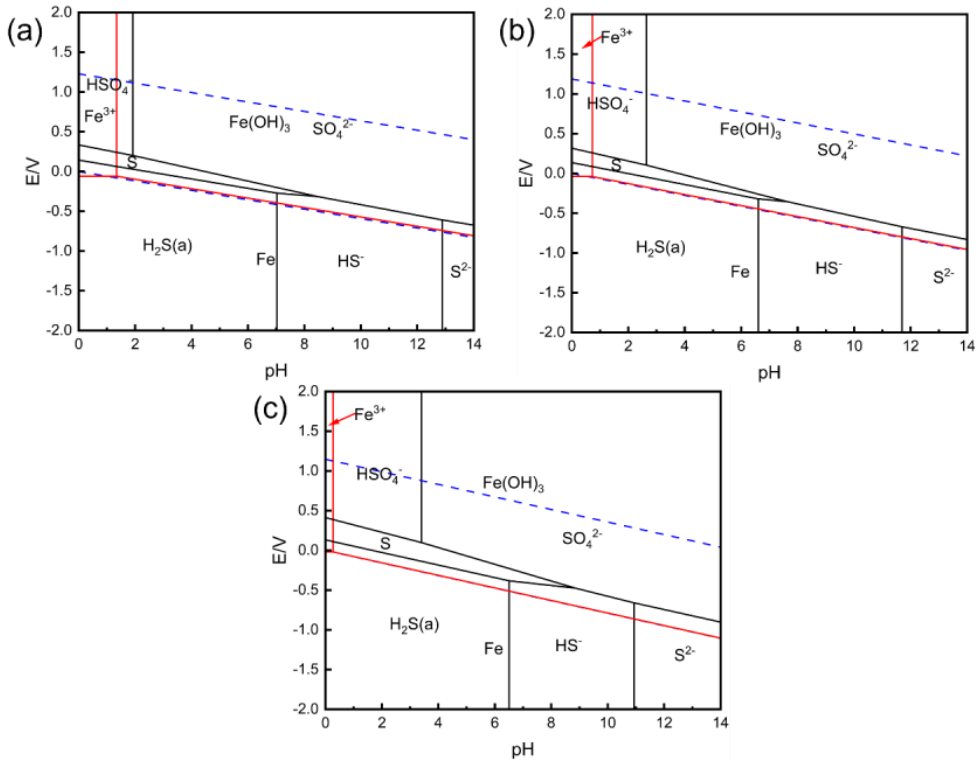

Figure 4. E-pH diagram of hydrolysis reactions in Fe-H_2SO_4-H_2O system at different temperatures. (a): 298 K, (b): 348 K, (c): 398 K.

At 298 K, Fe^{3+} remains stable within a pH range of 0–1.3. However, this stability window progressively narrows with increasing temperature, shrinking to pH 0–0.7 at 348 K and further to pH 0–0.3 at 398 K. Similarly, Figure 5 shows the E-pH diagrams for the Al-H_2SO_4-H_2O system, revealing that the maximum pH values for Al^{3+} stability decrease from 3.8 at 298 K to 2.8 at 348 K and 2.0 at 398 K.

This temperature-dependent behaviour stems from two fundamental factors:

- the hydrolysis of Fe^{3+} and Al^{3+} is endothermic, requiring heat absorption. Elevated temperatures promote greater heat uptake, thereby enhancing hydrolysis.
- according to Le Chatelier's principle, heating shifts the equilibrium of endothermic reactions toward product formation. In this context, increased temperature drives the hydrolysis equilibrium toward greater production of $Fe(OH)_3$ and $Al(OH)_3$.

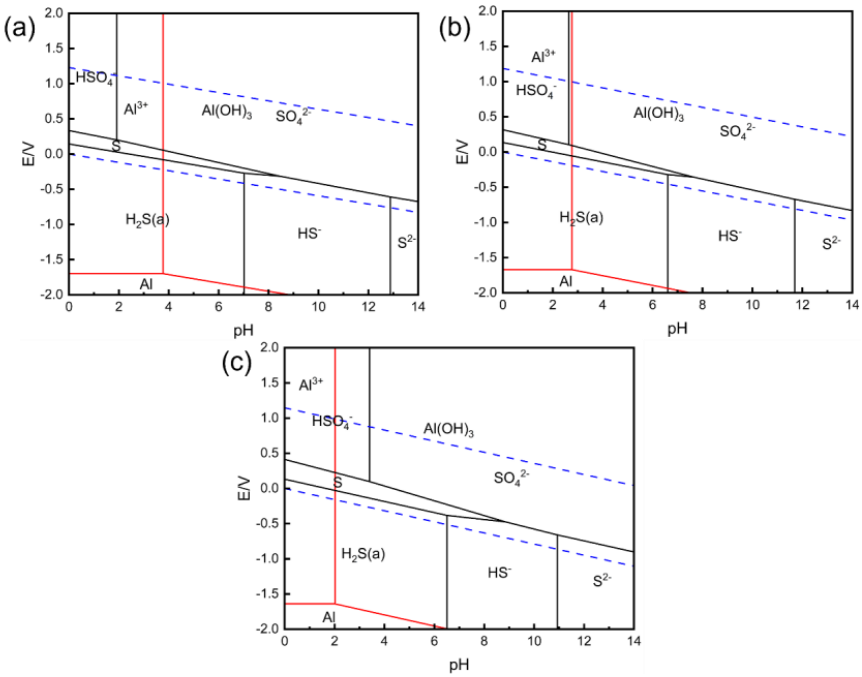

Figure 5. E-pH diagram of hydrolysis reactions in Al-H_2SO_4-H_2O system at different temperatures. (a): 298 K, (b): 348 K, (c): 398 K.

These findings highlight the critical need for precise pH control during the leaching process, particularly at higher temperatures where the stability ranges of Fe^{3+} and Al^{3+} become increasingly constrained. The results provide quantitative guidance for maintaining target metal ions in solution and preventing undesirable precipitation during hydrometallurgical processing of high-alkalinity red mud.

When CaO comes into contact with the dilute sulfuric acid leaching agent, the reaction begins at their interface. Calcium oxide is a basic oxide that can react with water to form $Ca(OH)_2$:

$$CaO + H_2O = Ca(OH)_2 \quad (5)$$

This reaction occurs immediately, as shown in the E-pH diagram (Figure 6), because calcium oxide readily reacts with water. The resulting $Ca(OH)_2$ subsequently reacts with dilute sulfuric acid to form calcium sulphate and water:

$$Ca(OH)_2 + 2H^+ + SO_4^{2-} = CaSO_4\downarrow + 2H_2O \quad (6)$$

Calcium sulfate ($CaSO_4$) has relatively low solubility in water and consequently precipitates as a solid phase. These precipitates form a passivation layer on the calcium oxide surface, creating a diffusion barrier that slows the reaction kinetics. However, the reaction persists through continuous exposure of fresh CaO surfaces to sulfuric acid. The process proceeds until either complete consumption of sulfuric acid or exhaustive conversion of calcium oxide to calcium sulphate and water occurs.

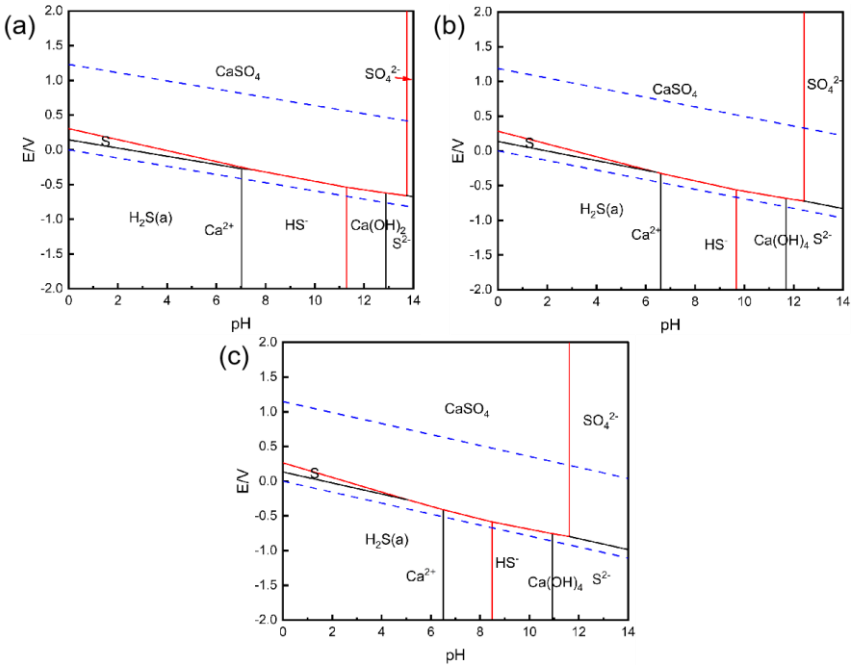

Figure 6. E-pH diagram of leaching reactions in Ca-H_2SO_4-H_2O system at different temperatures. (a): 298 K, (b): 348 K, (c): 398 K.

The solubility of silicon dioxide (SiO_2) during the leaching process is significantly influenced by both pH and temperature, exhibiting an increasing trend with rising pH and temperature. Figure 7 illustrates the existing forms of SiO_2 in the leaching system under different temperature conditions. The results demonstrate that SiO_2 cannot remain stable in the sulfuric acid leaching system. At leaching temperatures of 298 K and 348 K, silicon exists predominantly as orthosilicic acid (H_4SiO_4 or $Si(OH)_4$) under acidic conditions. When the temperature reaches 398 K, the primary form transitions to metasilicic acid (H_2SiO_3). Orthosilicic acid, a weak tetrabasic acid, exhibits unstable characteristics and limited solubility. Its molecules may undergo polymerization to form stable colloidal solutions, as represented by Reaction (7).

$$xH_4SiO_4 \rightarrow SiO_2 \cdot yH_2O \quad (7)$$

During the leaching process, silica gel increases the viscosity of the solution, resulting in poor fluidity and difficult filtration (consistent with observations in conventional leaching tests), while exhibiting strong adsorption capacity.

3.2 Kinetic Analysis

3.2.1 The Effect of Reaction Temperature

Investigating the effect of reaction temperature on leaching efficiency allows for estimation of the apparent activation energy, thereby determining the kinetic model and rate-limiting step of the leaching process. Under optimized conditions (sulfuric acid concentration: 0.8 mol/L; solid-to-liquid ratio: 1:4; stirring speed: 300 rpm), the influence of leaching time on sodium extraction efficiency was examined at different temperatures (298 K, 323 K, 348 K). The results are presented in Figure 8.

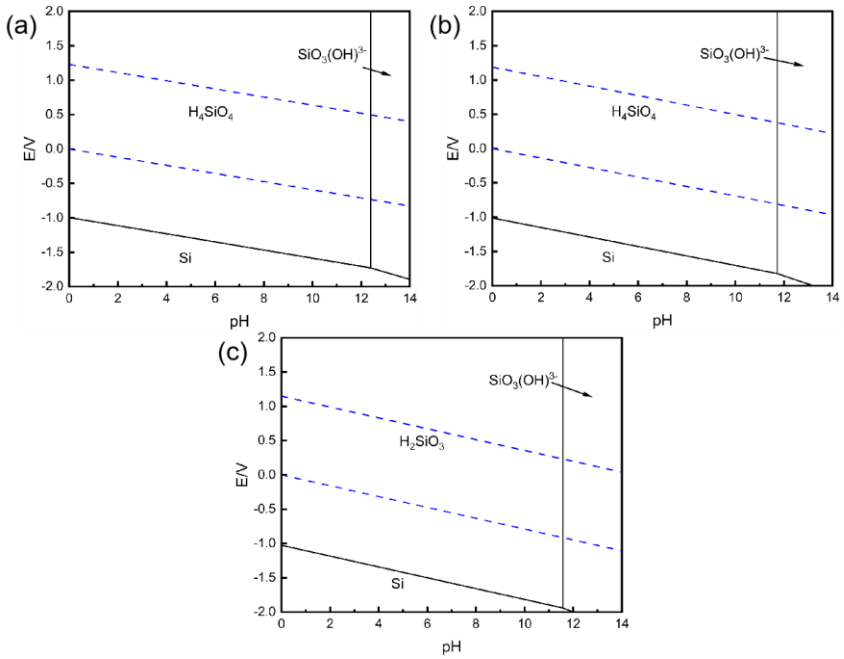

Figure 7. E-pH diagram of Si-H_2SO_4-H_2O system at different temperatures. (a): 298 K, (b): 348 K, (c): 398 K.

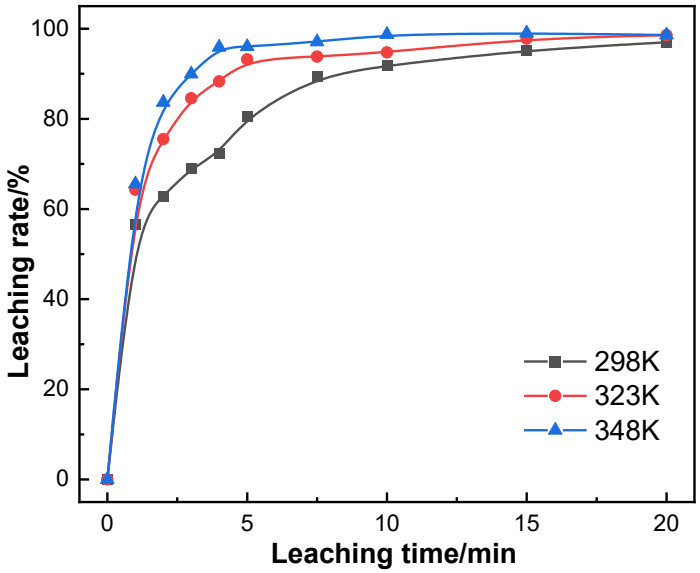

Figure 8. The variation curve of sodium leaching rate with reaction time at different reaction temperatures.

As shown in Figure 8, at 298 K the sodium leaching efficiency reaches 91.88 % after 10 minutes and increases to 96.96 % after 20 minutes. This indicates that at 298 K, the sodium leaching efficiency rapidly increases to a relatively high value within 10 minutes, with little further change upon prolonged leaching time.

At 323 K, the leaching efficiency quickly reaches 93.17 % within the first 5 minutes. When the leaching time is extended from 5 to 20 minutes, the efficiency only increases slightly from 93.17 to 98.55 %. Similarly, at 348 K, the leaching efficiency attains 96 % after just 5 minutes and merely increases to 98.6 % after 20 minutes. These results demonstrate that at both 323 K

and 348 K, the sodium leaching efficiency rapidly reaches a high value within 5 minutes, with minimal improvement upon further extension of leaching time.

In summary, most sodium-containing compounds in the red mud essentially complete their reactions with sulfuric acid under the following conditions: 5 minutes at either 323 or 348 K, or 10 minutes at 298 K. Although increasing temperature and prolonging leaching time can further enhance sodium extraction efficiency, the remaining sodium content in the red mud becomes very low and the leaching efficiency shows little change. Considering the substantial energy consumption and higher costs associated with elevated temperatures, the optimal leaching conditions for achieving efficient dealkalization at relatively low cost are determined to be 298 K for 10 minutes.

3.2.2 Kinetic Calculation

The leaching process is not considered to be diffusion-controlled. Assuming the mineral particles are approximately spherical, the reaction rate during leaching may be controlled by one of the following dominant mechanisms: internal diffusion control, chemical reaction control, or mixed control. Their respective expressions are as follows:

$$1 + 2(1-x) - 3(1-x)^{2/3} = k_1 t \quad (8)$$

$$1-(1-x)^{1/3} = k_2 t \quad (9)$$

$$1/3\ln(1-x) - 1 + (1-x)^{-1/3} = k_3 t \quad (10)$$

where:

x	leaching efficiency of valuable metals, %
t	leaching time, min
k_1	apparent rate constant for internal diffusion control
k_2	apparent rate constant for chemical reaction control
k_3	apparent rate constant for mixed control.

Based on the sodium leaching data from red mud under different temperatures and leaching times shown in Figure 8, and in conjunction with the three model equations for internal diffusion control, chemical reaction control, and mixed control, the dominant reaction mechanism governing the leaching process was determined. Using Equations (8), (9), and (10), linear regression analysis was performed between leaching time and leaching efficiency. The slopes of the fitted lines represent the apparent reaction rate constants k_1, k_2, and k_3, respectively. The applicability of each model was evaluated based on the correlation coefficient (R^2) of the linear fits. The results are presented in Figures 9–11.

The results demonstrate that across all three temperatures examined, the mixed control model [$1/3\ln(1-x)-1+(1-x)^{-1/3}$] provides the best fit to the experimental data, while the chemical reaction control model [$1-(1-x)^{1/3}$] shows the poorest correlation. Specifically, at 298 K, the correlation coefficients (R^2) for the three models are 0.898, 0.809, and 0.991 respectively. These findings clearly indicate that during the leaching process (0–20 min), the kinetic behaviour is most accurately described by the function $1/3\ln(1-x)-1+(1-x)^{-1/3}$, suggesting the process is predominantly governed by mixed control mechanisms where both internal diffusion and chemical reaction simultaneously influence the overall rate.

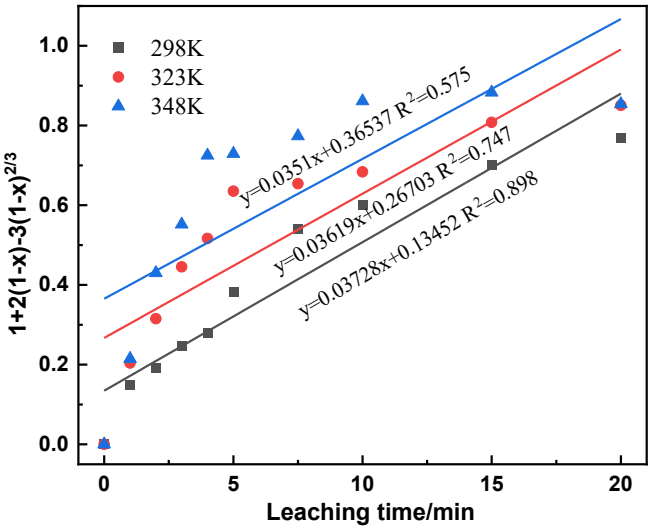

Figure 9. The fitting results of $1+2(1-x)-3(1-x)^{2/3}$ and leaching time.

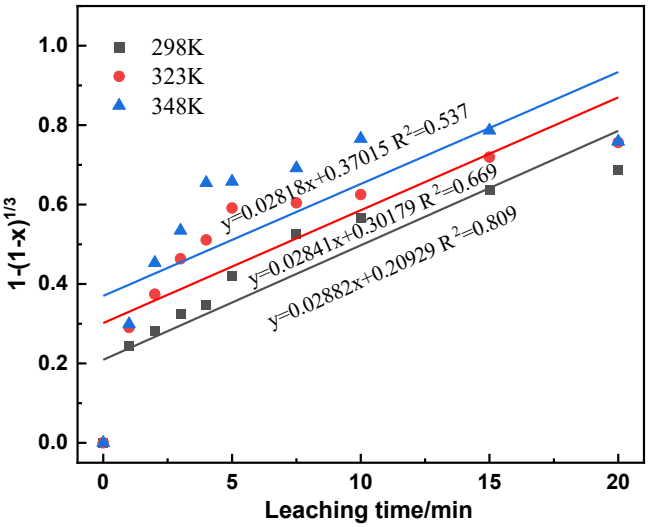

Figure 10. The fitting results of $1-(1-x)^{1/3}$ and leaching time.

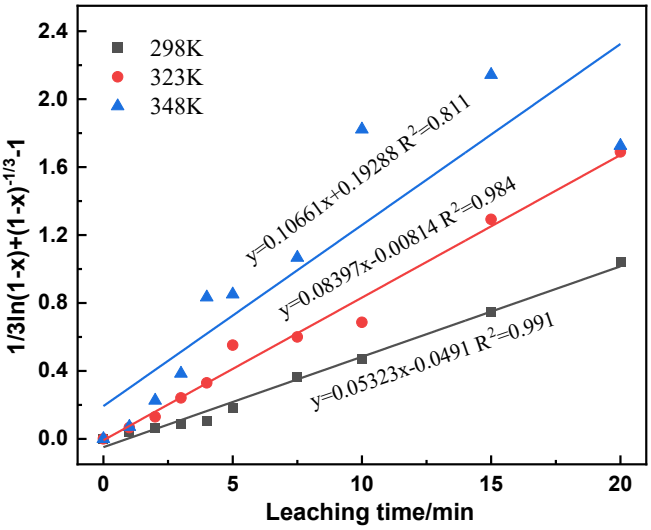

Figure 11. The fitting results of $1/3\ln(1-x)-1+(1-x)^{-1/3}$ and leaching time.

3.2.3 Calculation of Apparent Activation Energy

The apparent activation energy is one of the key characteristics for determining the rate-controlling step in leaching kinetics, which can be used to identify the controlling mechanism and develop methods for enhancing leaching rates. According to literature reports, when the activation energy exceeds 42 kJ/mol, the leaching process is generally controlled by the chemical reaction rate at mineral particle surfaces. For activation energies between 4 and 12 kJ/mol, the process is typically governed by diffusion rates through either the solid product layer or the solution boundary layer. When the activation energy falls within the range of 12–42 kJ/mol, the leaching process is usually subject to mixed control by both diffusion and chemical reaction rates. The apparent activation energy is calculated using the Arrhenius equation, which primarily reflects the relationship between the reaction rate constant (k) and leaching temperature (T), as expressed by the following formula:

$$k = Ae^{-E_a/RT} \tag{11}$$

where:

A frequency factor, min^{-1}
R ideal gas constant, 8.314 J/mol·K
Ea apparent activation energy, J/mol
T reaction temperature, K.

By taking the logarithm of both sides of formula (11), we obtain:

$$\ln k = \ln A - E_a/RT \tag{12}$$

According to the leaching reaction rate constant k_3 at different temperatures in formula (12), we can plot the relationship between ln(k) and 1/T at different temperatures and perform linear fitting. Then it is possible to calculate the apparent activation energy through the slope. The results are shown in Figure 12.

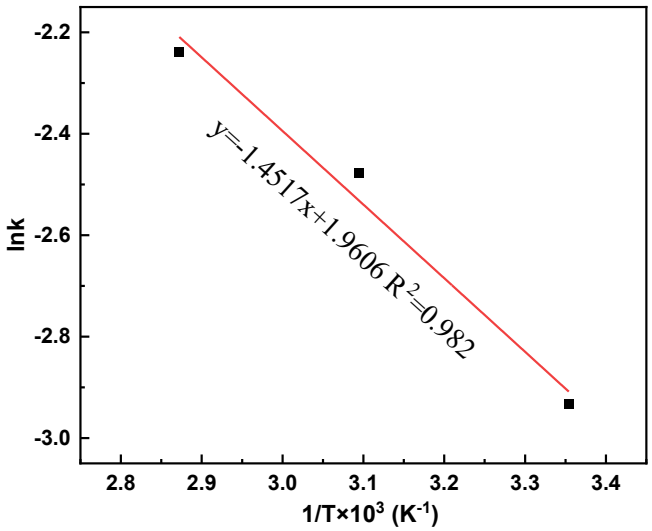

Figure 12. The Arrhenius plots for leaching kinetics of red mud.

As shown in Figure 12, the linear fitting between ln(k) and 1/T at different temperatures demonstrates good correlation, with a fitting correlation coefficient R^2 of 0.982. Based on this analysis, the apparent activation energy for sodium leaching from red mud was calculated to be

12.07 kJ/mol, indicating that the sodium leaching process is predominantly controlled by mixed mechanisms: both diffusion and chemical reactions.

4. Conclusions

Thermodynamic and kinetic analyses systematically elucidate the leaching behaviour of high-alkalinity red mud. Thermodynamic calculations reveal distinct temperature dependencies: the ΔG_T° values for Fe_2O_3 and Al_2O_3 leaching increase with temperature, becoming positive above 309 K, while Na_2O and CaO exhibit decreasing ΔG_T° trends. Notably, Na_2O demonstrates the most negative ΔG_T^θ values, indicating its preferential leaching tendency. These thermodynamic insights suggest that controlling temperature (> 323 K) and pH (4.0-7.0) can selectively extract Na_2O while suppressing Fe/Al dissolution.

Kinetic investigations demonstrate that approximately 90 % sodium extraction can be achieved within 5-10 minutes across 298 K-348 K. The leaching kinetics are best described by the mixed control model $[1/3\ \ln(1-x) - 1 + (1-x)^{-1/3}]$, showing excellent correlation superior to pure chemical reaction or diffusion models. This mixed control mechanism is further confirmed by the calculated apparent activation energy of 12.07 $kJ \cdot mol^{-1}$, which falls within the characteristic range for combined diffusion-chemical reaction control. The comprehensive understanding of both thermodynamic and kinetic aspects provides a scientific basis for optimizing the leaching process to achieve efficient and selective sodium extraction from high-alkalinity red mud.

5. References

1. F. Lyu, et al., Preliminary assessment of revegetation potential through ryegrass growing on bauxite residue, *Journal of Central South University*, Vol. 26, No. 2, 2019, 404–409.
2. X. Liu and N. Zhang, Utilization of red mud in cement production: a review, *Waste management & research*, Vol. 29, No. 10, 2011, 1053–1063.
3. D.-Y. Liu & C.-S. Wu, Stockpiling and comprehensive utilization of red mud research progress, *Materials*, Vol. 5, No. 7, 2012, 1232–1246.
4. E. Mukiza, et al., Utilization of red mud in road base and subgrade materials: A review, *Resources, conservation and recycling*, Vol. 141, 2019, 187–199.
5. I. Ghosh, et al., Leaching of metals from fresh and sintered red mud, *Journal of hazardous materials*, Vol. 185, No. 2-3, 2011, 662–668.
6. D. A. Rubinos & M. T. Barral, Fractionation and mobility of metals in bauxite red mud, *Environmental Science and Pollution Research*, Vol. 20, 2013, 7787–7802.
7. R. A. Pepper, et al., Comprehensive examination of acid leaching behaviour of mineral phases from red mud: Recovery of Fe, Al, Ti, and Si, *Minerals Engineering*, Vol. 99, 2016, 8–18.
8. F. Zhu, et al., Natural plant colonization improves the physical condition of bauxite residue over time, Environmental Science and Pollution Research, Vol. 23, 2016, 22897–22905.
9. W. Liu, et al., Application of Bayer red mud for iron recovery and building material production from alumosilicate residues, *Journal of hazardous materials*, Vol. 161, No. 1, 2009, 474–478.
10. F. Zhu, et al., Effects of iron-aluminium oxides and organic carbon on aggregate stability of bauxite residues, *Environmental Science and Pollution Research*, Vol. 23, 2016, 9073–9081.
11. X. Wang, et al., A novel utilization of Bayer red mud through co-reduction with a limonitic laterite ore to prepare ferronickel, *Journal of Cleaner Productio*n, Vol. 216, 2019, 33–41.
12. C. Klauber, et al., Proposed mechanism for the formation of dust horizons on bauxite residue disposal areas, *Essential Readings in Light Metals*: Volume 1 Alumina and Bauxite, 2016, 951–956.

13. X. Kong, et al., Acid transformation of bauxite residue: conversion of its alkaline characteristics, *Journal of hazardous materials*, Vol. 324, 2017, 382–390.
14. W. Mayes, et al., Advances in understanding environmental risks of red mud after the Ajka spill, Hungary, *Journal of sustainable metallurgy*, Vol. 2, 2016, 332–343.
15. C. Dickinson and G. Heal, Solid–liquid diffusion controlled rate equations, *Thermochimica Acta*, Vol. 340, 1999, 89–103.
16. X. Yang, et al., Rare earth element recycling from waste nickel-metal hydride batteries, *Journal of hazardous materials*, Vol. 279, 2014, 384–388.